Band offsets and band bending at heterovalent semiconductor interfaces

A. Frey, U. Bass, S. Mahapatra, C. Schumacher, J. Geurts, and K. Brunner
Physikalisches Institut (EP3), Universität Würzburg, Am Hubland, 97074 Würzburg, Germany

(Received 26 July 2010; published 16 November 2010)

We present a comprehensive study of band offsets and band bending at heterovalent semiconductor heterointerfaces. A perfectly abrupt heterovalent interface is usually thermodynamically unstable, and atomic intermixing of materials with different numbers of valence electrons causes large variations in band offsets and local doping density, depending on the spatial arrangement of atoms at the interface. The studied prototypical II-VI/III-V semiconductor interfaces are *n*-doped ZnSe/GaAs (001) heterostructures with varied composition profiles close to the interface, which were realized by molecular-beam epitaxy with different amounts of Zn or Se predeposited on *n*-GaAs prior to *n*-ZnSe layer growth. The samples are characterized by temperature-dependent electrical transport across the interface, electrochemical capacitance-voltage profiling, Raman spectroscopy, and high-resolution x-ray diffraction. We find that the potential barrier in the conduction band at a Zn-rich *n*-ZnSe/*n*-GaAs interface is as high as 550 meV and it gradually decreases with Se predeposition down to about 70 meV. A large depletion region at the heterointerface, about 50 nm wide, is assigned to significant intermixing of acceptor-type atoms, resulting in an effective electron deficit of 1.5×10^{13} cm^{-2}. The depletion width and the acceptor density around the interface are nearly independent from the growth start procedure. Se predeposition, however, partially shifts the depletion region at the heterointerface from GaAs into ZnSe, compared to Zn predeposition. The results are discussed on the basis of a band-bending model accounting for variable band offsets, interface state density and atomic interdiffusion profiles depending on growth start.

DOI: 10.1103/PhysRevB.82.195318 PACS number(s): 73.40.Lq, 73.61.Ga, 61.72.uj

I. INTRODUCTION

At isovalent semiconductor heterointerfaces, such as GaAs/AlAs or Si/Ge, the chemical band offsets, interface states, and doping levels completely determine the alignment and bending of the band edges. The electronic properties of *heterovalent* heterointerfaces, such as GaAs/Ge or ZnSe/GaAs, however, are additionally influenced by acceptor- and donor-type bonds across the interface.[1] A prototypical heterovalent material system is the II-VI/III-V semiconductor combination of ZnSe/GaAs, which has the advantage of closely matching lattice constants allowing for high-quality epilayers. At such an interface, Zn-As bonds lack 1/4 of an electron on average and act as acceptors while Se-Ga bonds have 1/4 excess electron and act as donors. The effect of these bonds is twofold: on the one hand, an excess of one type of bond over the other corresponds to *n*- or *p*-type planar doping, which can potentially be as high as 3.1×10^{14} cm^{-2}, see Ref. 2. Density-functional theory calculations show that such abrupt interfaces are thermodynamically unstable.[3] On the other hand, even if both are exactly balanced in number, their spatial arrangement on an atomic scale can lead to an electric dipole moment perpendicular to the heterointerface, which substantially affects and can even reverse the band offsets.[3] Applying photoelectron spectroscopy, Nicolini *et al.*[4] observed a variation in the valence-band offset (VBO) with the Zn/Se flux ratio employed during heteroepitaxy of ZnSe on GaAs (001). Furthermore, any atomic intermixing across a heterovalent interface implies doping of the adjacent layers, and thus affects the carrier distribution and band bending around the interface.[5–7]

The heterovalent ZnSe/GaAs (001) heterointerface has been studied extensively as part of the efforts to develop ZnSe-based optoelectronic devices. There the emphasis was mostly on reducing the density of structural defects originating from the heterointerface, in order to increase device lifetime.[8,9] It has been established[10–12] that avoiding the reaction of Se with the GaAs substrate surface by initiating ZnSe growth under Zn-rich conditions can yield defect densities as low as 10^3 cm^{-2}. More recently, this heterointerface has played a role in spin injection from ZnSe-based dilute magnetic semiconductors into GaAs (Refs. 13 and 14) and in optical studies of heterovalent coupled quantum wells in II-VI and III-V materials.[15,16] The functionality of such structures is very sensitive to band bending and band offsets at the ZnSe/GaAs interface.

In this paper we present a comprehensive study of the electronic and structural properties of heterovalent semiconductor heterointerfaces, and of the influence of different atomic composition profiles at the interface. As a representative material system we studied *n*-ZnSe/*n*-GaAs heterointerfaces prepared by molecular-beam epitaxy (MBE), and we varied the interface composition by predeposition of Zn or Se in the fractional monolayer (ML) range at ZnSe growth start. We find that the potential barrier height at the heterointerface can be changed over several hundred millielectron volts in a controllable fashion. We attribute this to a variation in the interface band offsets induced by electric dipole moments and of band bending induced by a redistribution of acceptors.

The growth start process was monitored by reflection high-energy electron diffraction (RHEED) and the structural quality of the epilayers was studied by high-resolution x-ray diffraction (HRXRD). Temperature-dependent current-voltage (*I*-*V*) measurements, electrochemical capacitance-voltage (ECV) measurements, and Raman spectroscopy are used to characterize the potential barrier and carrier density at the heterointerface.

 ©2010 The American Physical Society

TABLE I. Summary of fabricated samples with different ZnSe growth start (see Sec. III) and the results of structural, electrical, and Raman characterization. t is the ZnSe layer thickness obtained from HRXRD and $A_{\mathrm{diff}}/A_{\mathrm{layer}}$ is the ratio of diffusely scattered x-ray intensity to that under the ZnSe 004 Bragg peak. Φ_b is the potential barrier in the conduction band at the n-ZnSe/n-GaAs heterointerface determined by temperature-dependent I-V measurements, Σ is the areal electron deficit at the heterointerface obtained by integration of ECV profiles, $w_{\mathrm{d,ZnSe}}$ and $w_{\mathrm{d,GaAs}}$ are the individual depletion widths on the ZnSe and the GaAs side of the heterointerface, as determined by Raman spectroscopy.

Sample	Growth start	t (nm)	$A_{\mathrm{diff}}/A_{\mathrm{Layer}}$ (%)	Φ_b (meV)	Σ (10^{13} cm^{-2})	$w_{\mathrm{d,ZnSe}}$ (nm)	$w_{\mathrm{d,GaAs}}$ (nm)
A	20 s Zn, ALE	200	70	550 ± 150	1.6		
B	20 s Zn	242	23	470	1.1	20	26
C	7 s Se	232	9	300	1.9	50	15
D	11 s Se	219	5	280	1.4	41	16
E	15 s Se	207	24	73	1.3	37	16

The paper is organized as follows: after listing details of sample fabrication and measurements in Sec. II and describing the particular growth start procedures in Sec. III, the results of structural and electronic characterization are presented in Secs. IV and V, respectively. The results are discussed in Sec. VI in terms of a band-bending model including a varied conduction-band offset (CBO) and different distributions of acceptor states at or close to the heterointerface.

II. EXPERIMENTAL DETAILS

Samples were grown on epiready n-GaAs(001) ($N_{\mathrm{d}}=1-5\times10^{18}$ cm^{-3}) substrates by MBE in a system of interconnected III-V and II-VI chambers of the type Riber 32. Wafers were glued with In onto Mo sample holders and the substrate temperature was measured by a thermocouple in thermal contact with the Mo block. After growth of a 200-nm-thick n-GaAs buffer layer ($N_{\mathrm{d,GaAs}}=3\times10^{18}$ cm^{-3}) at 600 °C, the substrate was transferred to the II-VI chamber under ultrahigh vacuum, keeping an As-terminated, (2×4) reconstructed GaAs surface. In the II-VI chamber one of several growth start procedures was applied, as described in Sec. III. The II-VI part was grown at a substrate temperature of 300 °C and nominally consists of a 200 nm n-ZnSe ($N_{\mathrm{d,ZnSe}}=5\times10^{18}$ cm^{-3}) layer and a 30 nm n^+-ZnSe (2×10^{19} cm^{-3}) top contact layer. Si and ZnI_2 evaporated from effusion cells were used as n-type dopants in GaAs and ZnSe, respectively. Even though the total ZnSe layer thickness is close to the critical thickness for plastic relaxation in this material system, HRXRD confirms that all samples are pseudomorphic.

During ZnSe growth the Zn and Se beam equivalent pressures (BEPs) were 8×10^{-7} and 3×10^{-6} Torr, resulting in a growth rate of 1.2 Å/s and a (2×1) reconstructed surface. For Se predeposition a reduced Se BEP of 1×10^{-7} Torr was provided by opening the main shutter and leaving the Se cell shutter closed. Thereby the exposure time required for a Se coverage of 1 ML was increased from less than 1 s to about 18 s, allowing controllable submonolayer deposition by a meandering Se flux. The Se cell in our system was a valved cracker cell operated in the noncracking mode. During growth the sample surface was monitored by RHEED, using an electron beam energy of 12 keV.

For I-V measurements across the interface, (500 μm)^2 sized mesas were fabricated lithographically. Ohmic contacts to the n^+-ZnSe were prepared by *in situ* evaporated Al/Ti/Au and to the n-GaAs substrate by alloyed In on the backside. Temperature-dependent I-V curves were recorded using an HP 4145B parameter analyzer and a temperature-controlled helium flow cryostat. The ohmic nature of the metal/n^+-ZnSe contact was confirmed at 300 K and cryogenic temperatures. ECV was carried out using a BioRAD Polaron semiconductor profiler on samples whose *in situ* metallization was wet chemically removed before profiling. Raman investigations were performed utilizing an argon-ion laser (Coherent Innova 90, $h\nu=2.6$ eV) as excitation source and a SPEX double monochromator equipped with a multichannel detector as analyzer. The samples were cooled to liquid-nitrogen temperature in a cold-finger cryostat. HRXRD was done using a Panalytical X-Pert diffractometer equipped with a Cu $K_{\alpha1}$ source and a Ge analyzer crystal.

III. GROWTH START

Five samples named A to E have been fabricated using different ZnSe growth start procedures on As-terminated, (2×4) reconstructed GaAs(001) surfaces, as listed in Table I. The procedures differ in shutter sequences and substrate temperatures and aim at an increasing amount of Se at ZnSe growth start from sample A to E. In order to be able to detect any drift in growth conditions, the samples were grown in the sequence C, E, B, D, and A.

For sample A the substrate was exposed to Zn flux for 20 s at a low substrate temperature of 230 °C, then ZnSe growth was commenced in an atomic layer epitaxy (ALE) mode by alternately supplying Zn and Se flux while the substrate was ramped to the final growth temperature of 300 °C. After approximately 1 min this temperature was reached and growth was continued in MBE mode.

For sample B the substrate was exposed to Zn flux for 20 s as well but the starting temperature was 300 °C and ZnSe

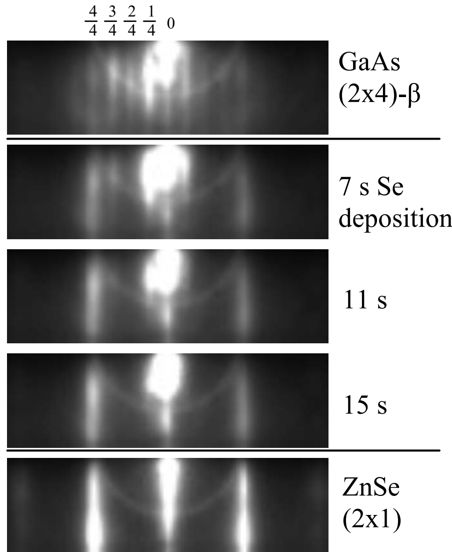

FIG. 1. RHEED patterns observed in the $[1\bar{1}0]$ azimuth before (top panel) and during Se predeposition (7–15 s). The bottom panel shows the pattern during ZnSe growth at about 15 nm layer thickness.

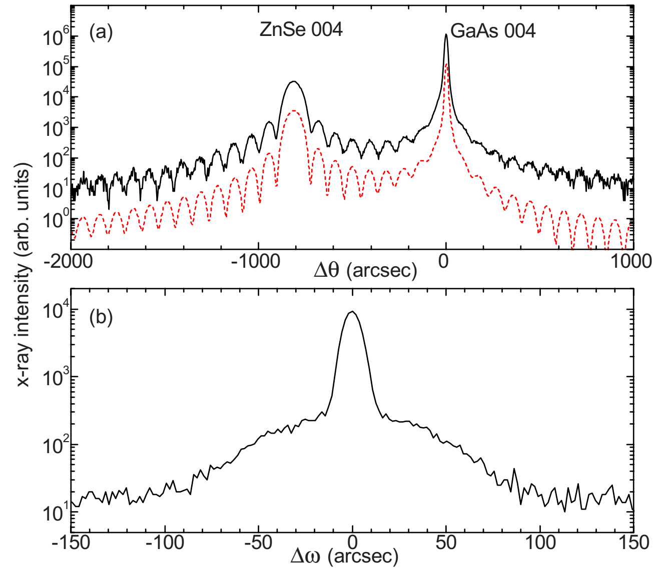

FIG. 2. (Color online) (a) HRXRD ω-2Θ scan in the vicinity of the 004 reflection of sample E (black solid line) and dynamic simulation (red dashed line). Curves are offset for clarity. (b) ω scan of the ZnSe 004 reflection of the same sample (x-ray beam is parallel to the 110 crystal direction), showing the narrow ZnSe Bragg peak and the broad, low intensity background peak which is attributed to diffuse scattering at dislocations.

growth was immediately commenced in MBE mode by opening the Se shutter. Due to the higher starting temperature and the consequently lower sticking coefficient of Zn, the ZnSe/GaAs interface formed by this growth start is expected to be slightly less Zn rich than for sample A. The initial (2×4) RHEED pattern does not change during Zn irradiation but a quick transition to a 2D (2×1) reconstructed surface was observed upon opening of the Se shutter.

For samples C, D, and E the substrate at 300 °C was exposed to the reduced Se BEP of 1×10^{-7} Torr at closed Se cell and open main shutter for different durations. Then ZnSe MBE growth was initiated by simultaneously opening the Zn and Se shutter.

During Se exposure RHEED showed a gradual transition from the initial (2×4) surface to an unreconstructed one, which was helpful in controlling the Se coverage. The RHEED patterns observed with the electron beam parallel to the $[1\bar{1}0]$ crystal direction are depicted in Fig. 1.

The top panel shows the GaAs (2×4) surface kept at 300 °C in the II-VI chamber with closed main shutter. Since the 2/4 streaks have about the same intensity as the other fractional order streaks, the surface can be more specifically assigned to type (2×4)-β, according to Ref. 17. The sample can be kept in this state for several minutes. Upon opening the main shutter and thereby applying a Se BEP of 1×10^{-7} Torr, the 2/4 order streaks weaken and disappear after 7 s. Then the 1/4 and 3/4 order streaks disappear after about 15 s, leaving an unreconstructed surface which does not change appreciably with further Se exposure. Samples C, D, and E were grown with Se predeposition for 7 s, 11 s, and 15 s, respectively.

A rough estimate of the Se coverage can be obtained from the deposition rate

$$R = \frac{p}{\sqrt{2\pi m k_B T}}. \quad (1)$$

With $p=10^{-7}$ Torr, $m=4\times79$ amu for Se_4, a cell temperature of $T=250$ °C, the Boltzmann constant k_B and assuming unity sticking coefficient, we get $R_{Se_4}=8.6\times10^{12}$ cm^{-2} s^{-1} or 0.8 ML of Se atoms deposited within 15 s (neglecting element-dependent pressure gauge sensitivity). We therefore ascribe the transition to an unreconstructed surface observed by RHEED to the deposition of Se in the fractional ML range. This is consistent with scanning tunneling microscopy results of Li and Pashley.[18]

IV. STRUCTURAL PROPERTIES

HRXRD scans of all samples have been measured in ω-2Θ and ω directions. Typical results are depicted in Fig. 2. For samples B to E HRXRD shows an 004 Bragg peak of a fully pseudomorphic ZnSe layer with more than ten thickness fringes in ω-2Θ direction [Fig. 2(a)]. The ZnSe 004 Bragg peak of sample A is slightly broadened and thickness fringes are less pronounced than for the other samples. From a fit of a calculated curve to the ω-2Θ scans we determined the ZnSe layer thickness as listed in Table I. We note that, although the growth duration and fluxes for all samples were identical, the ZnSe layer thickness decreases continuously with Se predeposition from 242 nm for sample B to 207 nm for sample E. The full width at half maximum (FWHM) of the ZnSe layer peak in ω direction [Fig. 2(b)] is about 10 arc sec for samples B to E, which is close to the resolution limit, and there is no significant broadening relative to

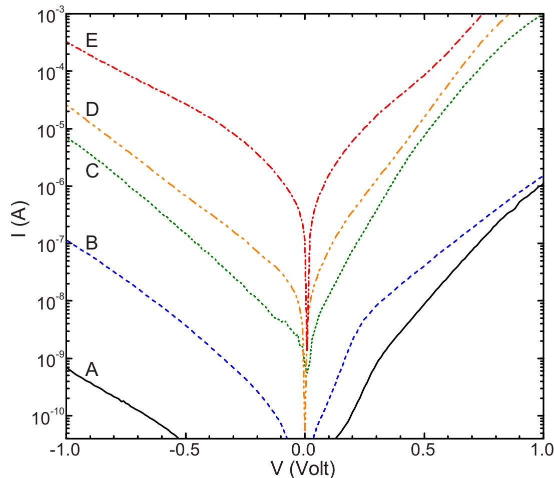

FIG. 3. (Color online) Room-temperature *I*-*V* characteristics measured through the *n*-ZnSe/*n*-GaAs heterointerface for samples A to E in (500 μm)^2 diodes. Positive bias corresponds to electron flow from ZnSe to GaAs.

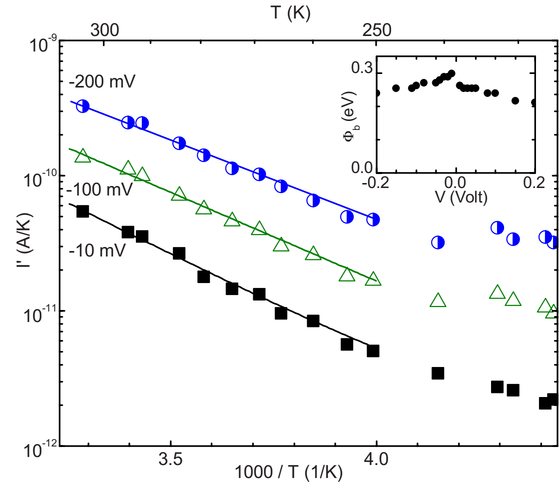

FIG. 4. (Color online) Arrhenius plot of the reduced current I' [definition see Eq. (2)] versus inverse temperature at different bias voltages for sample D. The interface barrier height Φ_b determined from the slope of I' is plotted in the inset as a function of bias.

the substrate peak. Thus the structural quality of these layers is very good and we find no sign of plastic relaxation. For sample A the ω FWHM is 20 arc sec, which, together with the slightly inferior ω-2Θ scan data, indicates that this sample is of lower structural quality. This may be due to a non optimized ALE start procedure for this sample.

A more sensitive HRXRD-based characterization of epitaxial layer quality has been demonstrated in Refs. 19 and 20. The intensity of the broad peak forming the background of an epilayer Bragg peak in the ω direction [Fig. 2(b)] is attributed to diffuse scattering from strained regions around dislocations. Thus, the ratio of integrated intensities of the diffusely scattered broad peak and the narrow Bragg peak from the epilayer is a sensitive measure of dislocation density. The intensity ratio is obtained by separately fitting Gaussian profiles to the diffuse and Bragg peak. The results for all samples are listed in Table I. Remarkably, samples with a moderate Se coverage at growth start have a lower dislocation density than those with Zn-rich growth start. For our highest Se coverage, however, the dislocation density increases sharply, as expected for growth on Se-rich surfaces.[11]

V. ELECTRONIC PROPERTIES

A. *I*-*V* characteristics

As a first measure of the electronic properties of the fabricated heterovalent heterointerfaces we analyze the room-temperature *I*-*V* characteristics measured across the interface in (500 μm)^2 mesas. The results are shown in Fig. 3. We first note that all *I*-*V* curves are non-ohmic, which indicates that electron transport is limited by a potential barrier. Second, the conductivity at a fixed bias voltage strongly depends on the ZnSe growth start procedure. There is a monotonic trend toward higher current density with increasing Se predeposition, which spans nearly 5 orders of magnitude. This indicates that the potential barrier limiting the current is situated at the heterointerface and that its height and/or width are reduced by Se predeposition. However, the resistance even of the best conducting samples is rather high. The differential resistance of sample E is 83 kΩ at 0 V while for purely diffusive transport the resistance would be <1 Ω. Third, we note that the *I*-*V* characteristics are asymmetric: when ZnSe is on negative potential with respect to GaAs the current is higher than in the opposite direction. The former polarity is denoted as $V>0$ (forward bias) in Fig. 3. This is consistent with a type-I band line up, in which the CB edge in ZnSe lies above that of GaAs (defined as positive CB offset). The asymmetry is very pronounced for samples A and B with a Zn-rich growth start and becomes much weaker with increasing Se predeposition.

For a quantitative measure of the heterointerface potential barrier, *I*-*V* curves are taken as a function of temperature in the thermionic emission regime. In this regime the following relationship between the "reduced current" I' and the applied bias voltage V holds for small bias voltages:[21]

$$I' = \frac{I}{T\left(\exp\left\{\dfrac{eV}{k_BT}\right\} - 1\right)} \propto \exp\left\{\frac{-\Phi_b}{k_BT}\right\} \qquad (2)$$

with the current I, the temperature T, the elementary charge e, and the Boltzmann constant k_B. In the model, which neglects tunneling, Φ_b is the potential barrier height in the conduction band measured from the Fermi energy. In the experiment, tunneling may reduce the energy needed for electrons to traverse the barrier so Φ_b rather corresponds to the activation energy for thermally activated tunneling. It corresponds to the absolute height but is also slightly influenced by the shape of the heterointerface potential barrier.

Φ_b can be determined from the slope of $\ln(I')$ when plotted over $1/T$ in an Arrhenius plot.[22,23] This is shown in Fig. 4 for sample D at different bias voltages. For $T>250$ K I' in

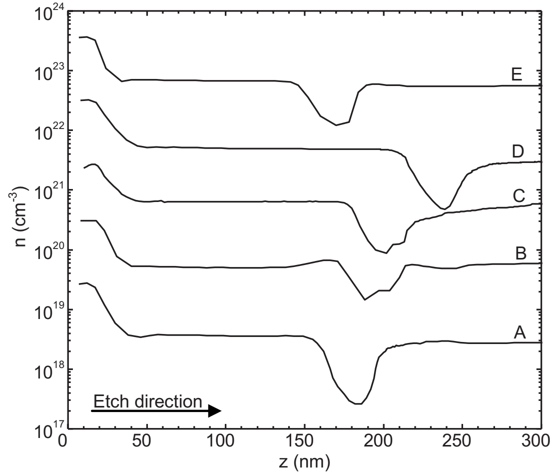

FIG. 5. Profiles of the electron density $n(z)$ obtained by ECV for samples A to E. The origin of the bottom axis corresponds to the ZnSe surface. Curves B to E are subsequently offset by 1 order of magnitude.

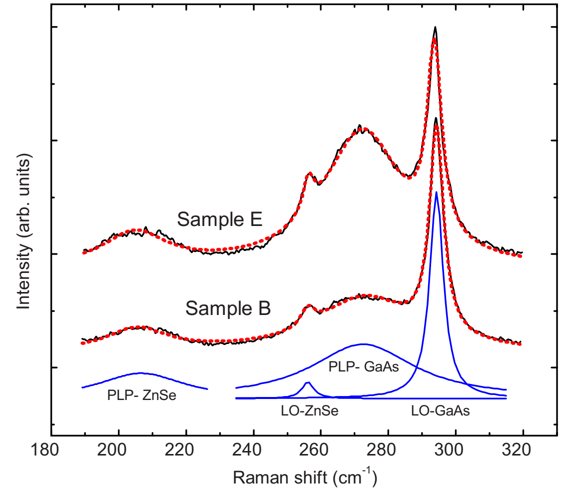

FIG. 6. (Color online) Exemplary Raman spectra of samples B and E, taken with an excitation wavelength of 477 nm (black solid curves). Each spectrum comprises the phonon peaks LO_{ZnSe} and LO_{GaAs}, originating from the carrier-depleted near-interface region, and the corresponding coupled plasmon-phonon modes PLP_{ZnSe} and PLP_{GaAs}, originating from the doped ZnSe epilayer and the underlying doped GaAs, respectively. Both spectra are fitted by a superposition of four Lorentz functions (red dotted curves). At the bottom, the Lorentz functions corresponding to the fit for sample B are shown individually.

Fig. 4 varies exponentially with inverse temperature, indicating the thermionic emission regime, and it becomes temperature independent at low temperatures where tunneling conduction dominates. The barrier height extracted from the slope in the exponential region is shown in the inset of Fig. 4 as a function of the applied bias. For each sample Φ_b was extrapolated to zero bias and the mean value of the extrapolation from the positive and negative side was taken as the final barrier height. In sample A, due to its high resistance and possibly also due to fluctuating barrier properties caused by structural defects, the barrier height could only be determined at higher applied bias voltages and with a relatively large uncertainty. As listed in Table I we find a high barrier of about 550 meV for the ALE growth start sample A, 470 meV for the conventionally grown Zn-rich sample B, and a monotonic reduction with Se predeposition, down to 73 meV for sample E. One of our main results is thus that Se predeposition drastically and controllably reduces the potential barrier in the conduction band at the n-ZnSe/n-GaAs heterointerface. It is remarkable that the bias dependence of the barrier height $\phi_b(V)$ of samples C to E with low barrier is rather symmetric, as shown exemplary in the inset of Fig. 4.

B. Carrier-density distribution

In Fig. 5 we show the electron-density profiles $n(z)$ of all samples measured by ECV at room temperature. Close to the surface, the 30 nm thick, 2×10^{19} cm^{-3} doped n^+-ZnSe top contact layer can be seen, followed by the 5×10^{18} cm^{-3} doped "bulk" n-ZnSe. At a depth corresponding approximately to the ZnSe/GaAs heterointerface there is an about 40–60 nm wide depletion region, after which the carrier density increases to the value intended for the n-GaAs buffer. We note that there is no electron accumulation on the GaAs side of the heterointerface. The scattering of the depth of the depletion region is mainly attributed to inaccuracy of the ECV etch rate. Integrating the difference between the donor density $N_{d,i}$ (i=ZnSe or GaAs), measured far away from the interface, and the electron density $n(z)$ across the interface region gives an integrated electron deficit $\Sigma=\int N_{d,i}-n(z)dz$. Evaluating this integral in the range $100\leq z\leq300$ nm for all measured profiles yields Σ in the range $1.1-1.9\times10^{13}$ cm^{-2}, as listed in Table I for the individual samples. We estimate experimental error bars for Σ of $\pm0.5\times10^{13}$ cm^{-2} based on the reproducibility of the measurements and on the uncertainty of the heterointerface position in ECV profiles. We thus find an average electron deficit $\Sigma=(1.5\pm0.5)\times10^{13}$ cm^{-2} at the studied heterovalent ZnSe/GaAs heterointerfaces with no significant variation with the growth start procedure. This electron deficit is often interpreted directly as the density of interface states.[24] In Sec. VI we will show that in these n-doped heterovalent samples it is not only due to interface states but also to an extended distribution of acceptors or to a lack of donors (e.g., due to segregation) over several tens of nanometer around the interface. Our measured value for Σ is in remarkable agreement with the results of Kassel *et al.*,[6] who found an areal density $1.0-1.5\times10^{13}$ cm^{-2} of interdiffused Zn acceptors in GaAs at ZnSe/GaAs heterointerfaces.

For the determination of the individual depletion layer width on each side of the ZnSe/GaAs interface, Raman spectroscopy was applied. As exemplary results, the spectra in Fig. 6 show the inelastic light scattering intensity of the samples B and E in the frequency range of the ZnSe and GaAs lattice vibrations. The peaks originate from the longitudinal-optical (LO) phonon modes ($\tilde{\nu}_{LO,ZnSe}=256$ cm^{-1} and $\tilde{\nu}_{LO,GaAs}=294$ cm^{-1}) and from the coupled plasmon-LO-phonon (PLP) modes, located at $\tilde{\nu}_{PLP,ZnSe}=207$ cm^{-1} and $\tilde{\nu}_{PLP,GaAs}=272$ cm^{-1}. They allow the individual determination of the depletion layer widths $w_{d,ZnSe}$

and $w_{d,GaAs}$ since only the depletion layers give rise to the LO phonons. From the doped ZnSe epilayer and the doped GaAs behind the interface the shifted peaks PLP_{ZnSe} and PLP_{GaAs} arise.[25] Thus, the distinction between both depletion layers is enabled by the intensities of the LO_{ZnSe} and LO_{GaAs} peaks. In ZnSe, the LO intensity is directly proportional to the $w_{d,ZnSe}$ since the regions with carriers instead emit coupled PLP modes at a different wave number. The ZnSe material is transparent for the laser light ($h\nu=2.6$ eV$<E_g=2.8$ eV). The value of $w_{d,ZnSe}$ is obtained after intensity calibration with an undoped ZnSe layer of well-known thickness. In the opaque GaAs ($E_g=1.5$ eV), light attenuation effects are considered because of the finite penetration depth $d_p=70$ nm (see Ref. 26). The straightforward procedure for the calculation of $w_{d,GaAs}$ is described in great detail in Ref. 27.

The exemplary spectra of the samples B (Zn start) and E (15 s Se predeposition) in Fig. 6 show clear differences. Sample B gives a strong LO_{GaAs} together with a rather weak LO_{ZnSe}. In contrast, in sample E LO_{GaAs} is reduced while LO_{ZnSe} and PLP_{GaAs} are enhanced. The fitting results, also shown in Fig. 6, yield an LO_{ZnSe} enhancement factor of 1.88 for sample E with respect to B. As explained above, the intensity of the LO_{ZnSe} peak is directly proportional to the width of the carrier depleted region in ZnSe. After intensity calibration we obtain for sample B and E the $w_{d,ZnSe}$ values of 20 nm and 37 nm, respectively. Considering the GaAs signals, for the Se predeposited sample the ratio of the depletion-induced LO_{GaAs} intensity and the doping-induced PLP_{GaAs} intensity amounts to $I_{LO}/I_{PLP}=0.20$, which means a considerable reduction with respect to the corresponding value for sample B, which is as high as 0.32. The evaluation of these results according to Ref. 27 yields $w_{d,GaAs}=26$ nm for sample B and $w_{d,GaAs}=16$ nm for sample E. For the other Se predeposited samples C and D we observe the same trend as for sample E. The corresponding depletion layer values are listed in Table I. Thus, throughout our sample series the determination of the individual depletion layer thicknesses $w_{d,ZnSe}$ and $w_{d,GaAs}$ by Raman spectroscopy reveals a partial shift of the depleted interface region from the GaAs side toward the ZnSe side with increasing Se predeposition.

As a third probe of the carrier density at the heterointerface we measured the capacitance of the mesa diodes already used for *I-V* measurements. Since, unlike in ECV measurements, the metal/semiconductor contacts in these samples are ohmic, their capacitance is determined only by the depletion region at the ZnSe/GaAs heterointerface. Accounting for possible parallel conductance of the mesas (especially for sample E), we measured capacitances in the range $C=289-348$ pF for all samples. In the total depletion approximation the capacitance is $C=\epsilon\epsilon_0 A/w_{d,total}$ with $A=(500\ \mu m)^2$ and $w_{d,total}$ being the total width of the carrier depleted region. The dielectric constant ϵ should be the appropriately weighted, harmonic mean between the ZnSe value $\epsilon_{ZnSe}=8.6$ and the GaAs value $\epsilon_{GaAs}=12.9$, reflecting the distribution of the depletion region between the two materials. When assuming equal depletion on both sides, $\epsilon=2/(1/\epsilon_{ZnSe}+1/\epsilon_{GaAs})=10.3$, depletion widths $w_{d,total}=65-78$ nm are obtained for all samples. This range for $w_{d,total}$ is in fair agreement with the sum of the individual depletion widths measured by Raman spectroscopy (Table I) and the depletion width in ECV profiles (Fig. 5). For the Se-start samples C to E the agreement of capacitance with Raman and ECV results is further improved when it is considered that the larger fraction of the depleted region is in ZnSe, and therefore ϵ is smaller. Differences between the depletion width results obtained by the three applied methods ECV, Raman and capacitance measurements, may be due to possible systematic errors and due to different limits to the electron density below which a layer appears as depleted.

VI. DISCUSSION

Our detailed results on depletion widths, carrier compensation, and potential barrier heights at the studied heterovalent interfaces obviously require a much more detailed description than merely determining the chemical band offset given by the materials. In order to develop a consistent picture of the electronic properties of the *n*-ZnSe/*n*-GaAs heterointerface, which accounts for the observed electronic properties and for their variation with predeposition of Zn or Se, we have considered band offsets as well as band bending and have calculated one-dimensional (1D) band and carrier-density profiles for different models of the heterointerface using a Poisson solver.[28] Material data for ZnSe and GaAs are taken from the literature,[29,30] and the donor density in ZnSe is $N_{d,ZnSe}=5\times10^{18}$ cm^{-3} and in GaAs $N_{d,GaAs}=3\times10^{18}$ cm^{-3}. Calculations are done for a temperature of 300 K. We assumed that all impurities are fully ionized, unless noted otherwise.

Each adequate description of heterovalent semiconductor interfaces requires the possibility of a variable band offset. This is in contrast to isovalent interfaces, whose electronic properties are determined by fixed VBO and CBO, and for which a low density of interface states and effects like interface roughness and atomic interdiffusion only smear out the band offset region, without changing the offset value. At *heterovalent* heterointerfaces such as ZnSe/GaAs, however, the band offsets can be varied significantly by an electric dipole moment perpendicular to the interface, which originates from the atomic arrangement of donor- and acceptor-type bonds across the interface. For ZnSe/GaAs, this contrasting behavior is visualized by comparing the nonpolar (110)-oriented interface with the polar one on (001) planes. While the VBO at a nonpolar ZnSe/GaAs (110) heterointerface is close to 1.1 eV, effective VBOs between 0.72 and 1.75 eV have been calculated for polar ZnSe/GaAs (100) heterointerfaces with different interface dipole moments (Ref. 3, and references therein). This range of VBOs implies CBOs between −0.45 and 0.58 eV, considering that the ZnSe band gap is $\Delta E_g=1.3$ eV wider than that of GaAs. The possibility of variable band offsets is thus included in three heterointerface models with increasing degree of sophistication concerning the acceptor state distribution, which are described in Secs VI A–VI C.

A. Model (a): Variable band offset and interface state density

In panel (a) of Fig. 7 the calculated Γ_6 CB diagrams and electron-density profiles are shown for *n*-ZnSe/*n*-GaAs het-

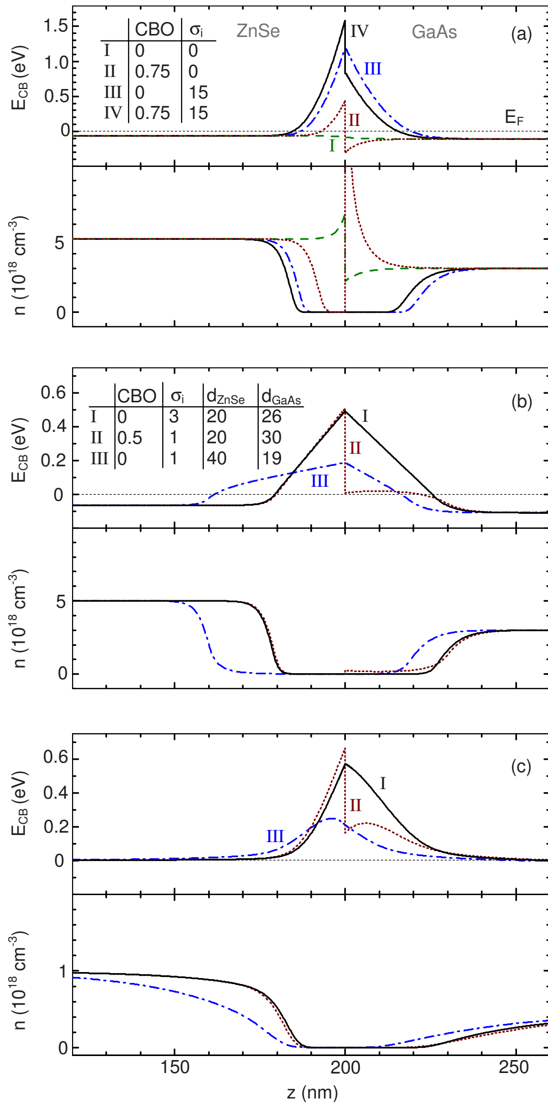

FIG. 7. (Color online) Calculated profiles of the CB edge E_{CB} and the electron density n in the conduction band for the three n-ZnSe/n-GaAs heterointerface models described in Sec. VI. In (a) only a CBO and an interface state density σ_i are considered, the parameters corresponding to the individual curves are listed in the inset (CBO in electron volt and σ_i in 10^{12} cm^{-2}). In (b) the effects of atomic interdiffusion and segregation are included by assuming exactly compensated regions of width d_{ZnSe} and d_{GaAs} on the two sides of the heterointerface (both given in nanometer in the inset). In (c) such effects are modeled by an exponentially varying n- or p-type doping density at the interface, the parameters corresponding to the curves are listed in Table II. Incomplete ionization of impurities is allowed only in (c). The temperature is 300 K and the interface is situated at z_i=200 nm. Note the different scale of E_{CB} in (a) compared to (b) and (c), and of n in (c) compared to (a) and (b).

erointerfaces with CBO=0 eV (curve I) and CBO =0.75 eV (curve II). A finite CBO causes a barrier in the conduction band, electron depletion in ZnSe, and accumulation in GaAs. Even though barrier heights comparable to those observed in this work can be easily caused by a CBO in the range predicted in the literature,[3] the corresponding electron-density profiles are in obvious disagreement with our results, as we observe no electron accumulation in GaAs but an integrated electron deficit $\Sigma = 1.5\times10^{13}$ cm^{-2}. Accounting for this deficit with an interface state density $\sigma_i = 1.5\times10^{13}$ cm^{-2} together with CBO=0 (curve III) or with CBO=0.75 eV (curve IV) in both cases yields electron-density profiles that are in better agreement with our measured profiles. Even for a CBO as large as 0.75 eV there is no electron accumulation on the GaAs side and the total width of the depleted region is in fair agreement with the experimental results. However, this model results in potential barriers of more than 1 eV, much larger than measured in this work. Lower barriers can only be explained by assuming that Σ is not only caused by a two-dimensional interface state density but by acceptors distributed over several tens of nanometer around the interface. This is in agreement with our previous work, in which we have found evidence for an exceptionally large depletion region at n-ZnSe/GaAs heterointerfaces.[7] Effects leading to such a spatial extension of the depletion region are compensation of n doping due to atomic interdiffusion across the heterointerface,[5] dissolution, and segregation of As atoms from the As-terminated GaAs surface at growth start, and segregation of iodine donors in ZnSe during MBE deposition.

B. Model (b): Interdiffusion and segregation modeled with box-shaped doping profiles

The simulations in panel (b) include such a spatially extended electron deficit by assuming exact compensation of donors with acceptors of the density $N_a = N_d$ in a region of width d_{ZnSe} in ZnSe and d_{GaAs} in GaAs at the heterointerface. The integrated electron deficit in the interface region is then

$$\Sigma = \sigma_i + d_{ZnSe}\cdot N_{d,ZnSe} + d_{GaAs}\cdot N_{d,GaAs} \tag{3}$$

with the nominal bulk donor densities $N_{d,ZnSe}$ and $N_{d,GaAs}$. Outside this box-shaped region the donor density equals the bulk values in the two materials. This assumption of an exactly compensated region with abrupt transition to homogeneously doped bulk layers on both sides of the heterojunction may seem arbitrary but the exact doping density profiles are not central to our discussion at this point. A more realistic model is described in Sec. VI B. Together with a variable CBO and σ_i the model thus includes four parameters, which have been adjusted so that the resulting CB and carrier-density profiles agree with the measured quantities Φ_b, $w_{d,ZnSe}$, $w_{d,GaAs}$, and Σ for samples B and E, representing Zn-rich and Se-rich growth start, respectively.

Curves I and II are both consistent with the experimental results for sample B. Curve I is calculated with a vanishing CBO and a relatively high $\sigma_i = 3\times10^{12}$ cm^{-2} while curve II is calculated for a high CBO=0.5 eV and a low $\sigma_i = 1\times10^{12}$ cm^{-2}. For curve I we use d_{ZnSe}=20 nm and d_{GaAs}=26 nm, and for curve II d_{ZnSe}=20 nm and d_{GaAs}=30 nm. Since both parameter sets equally well reproduce all four measured electronic interface properties within their respective uncertainties, answering the question of whether a high CBO or a high interface state density produces the observed potential barrier in the Zn-rich samples requires additional

experimental information. We find such information in the asymmetry of the *I-V* curves (Fig. 3): a symmetric barrier is lowered nearly equally by an applied voltage independent of the polarity of the voltage, and thus the resulting *I-V* characteristics are nearly symmetric. An asymmetric barrier caused by a large CBO, on the other hand, is only lowered if the material with the higher lying CB edge is on negative potential, while for the other bias direction always a finite, nearly triangular barrier remains. The *I-V* characteristics of such a barrier is also asymmetric with the forward bias direction corresponding to the material with the higher CB edge energy being on negative potential. Thus the markedly asymmetric *I-V* characteristics especially of samples A and B indicates that the observed high interface barrier for those samples is asymmetric and is caused by a substantial CBO.

Curve III is an adaptation to sample E and is calculated with CBO=0 eV, $\sigma_i = 1\times10^{12}$ cm^{-2}, $d_{\mathrm{ZnSe}}=40$ nm, and $d_{\mathrm{GaAs}}=19$ nm. In order to obtain a low potential barrier obviously both the CBO and σ_i need to be relatively low. The resulting potential barrier is rather symmetric and thus is consistent with the low asymmetry of *I-V* curves (Fig. 3) and of the bias dependence of the barrier heights (inset of Fig. 4). For all simulations in panel (b) Σ is in the range $2-3\times10^{13}$ cm^{-2}, which is in fair agreement with the value derived from ECV profiles. Thus we have shown that the measured electronic interface properties Φ_b, $w_{\mathrm{d,ZnSe}}$, $w_{\mathrm{d,GaAs}}$, Σ and the degree of asymmetry in the *I-V* curves can be consistently explained with a model including a variable CBO and σ_i, and using box-shaped doping profiles to account for extended depletion regions at the interface. The reduction in the interface potential barrier with Se predeposition is ascribed mainly to a reduction in the CBO, based on a qualitative evaluation of the asymmetry of *I-V* curves.

C. Model (c): Interdiffusion and segregation modeled with continuous doping profiles

In panel (c) we show calculated band and electron-density profiles based on a physically more intuitive model, where we assume exponentially decaying acceptor and donor densities instead of the box-shaped ones in model (b), and allow for incomplete ionization of impurities at 300 K. Interdiffusion of acceptor type atoms in ZnSe and in GaAs is modeled as an exponentially decreasing acceptor density,

$$N_{\mathrm{a},i}(z) = N_{0,i}\exp\left\{\frac{-|z-\hat{z}|}{\lambda_i}\right\}, \quad (4)$$

where i=ZnSe or GaAs, $\hat{z}$ is the interface position and $N_{0,i}$ and λ_i correspond to the saturation density and diffusion length of interdiffused atoms. Furthermore, delayed incorporation of iodine donors in ZnSe ($z<\hat{z}$) due to segregation is modeled as

$$N_{\mathrm{d}}(z) = N_{\mathrm{d,ZnSe}}\left(1-\exp\left\{\frac{-|z-\hat{z}|}{k}\right\}\right) \quad (5)$$

with $N_{\mathrm{d,ZnSe}}$ being the nominal bulk donor density in ZnSe and k corresponding to the segregation length. The integrated electron deficit is

TABLE II. Parameter sets used for the three simulations depicted in panel (c) of Fig. 7.

	I	II	III
CBO (eV)	0	0.5	0
σ_i (10^{12} cm^{-2})	3	1	0
$N_{0,\mathrm{GaAs}}\cdot\lambda_{\mathrm{GaAs}}$ (10^{12} cm^{-2})	10	12.5	6.2
λ_{GaAs} (nm)	20	20	20
$N_{0,\mathrm{ZnSe}}\cdot\lambda_{\mathrm{ZnSe}}$ (10^{12} cm^{-2})	0	0	7.5
λ_{ZnSe} (nm)	0	0	25
k (nm)	25	25	25

$$\Sigma = \sigma_i + N_{0,\mathrm{ZnSe}}\cdot\lambda_{\mathrm{ZnSe}} + N_{0,\mathrm{GaAs}}\cdot\lambda_{\mathrm{GaAs}} + k\cdot N_{\mathrm{d,ZnSe}}. \quad (6)$$

As done for model (b), we adjust the model parameters to give band and electron-density profiles which best fit the measured electrical interface properties. The resulting profiles for sample B and E are shown in panel (c) of Fig. 7 and the corresponding model parameters are listed in Table II. Due to incomplete ionization the electron density n in the conduction band is lower than the donor density $N_{\mathrm{d},i}$. Such a lower electron density is in good agreement with the PLP mode frequencies observed by Raman and infrared spectroscopy (not shown here).

The Zn-rich sample B can be described by a vanishing CBO and a relatively large interface state density σ_i (curve I), resulting in a nearly symmetric barrier, as well as by a large CBO=0.5 eV and a smaller σ_i (curve II), resulting in an asymmetric barrier. As explained in (b) only the latter is consistent with the shape of the *I-V* curves. Such a large CBO has been predicted in Ref. 3 for an atomic interface configuration with a pure Zn plane and a subjacent mixed anionic plane with a composition of 50% As and 50% Se. This interface fulfills the charge neutrality condition (neglecting a small σ_i) and is the most stable of the configurations calculated in Ref. 3.

For the Se-rich growth start sample E (curve III), the CBO and σ_i both have to be small. A systematic parameter variation in our model calculations shows that the observed small potential barrier $\Phi_b=73$ meV limits the possible values of model parameters to about CBO<0.1 eV and $\sigma_i < 2\times10^{12}$ cm^{-2}. A small interface state density σ_i may be explained considering that predeposition of Se on GaAs leads to some donor-type Ga-Se bonds, which partially compensate acceptor-type interface states. A small CBO is related to the formation of a heterointerface with a vanishing electric dipole moment, as it was calculated in Ref. 3 for interfaces with two mixed atomic planes. The (2×2) interface containing a mixed anionic plane with 75% Se and 25% As on top of a cationic plane with 25% Zn and 75% Ga has a CBO as low as 80 meV, in agreement with our measurements, and a rather high stability.[3] It contains a high proportion of Se at the heterointerface and thus is reasonable for an interface formed by Se predeposition. This high Se concentration may stabilize Zn atoms incorporated in the cationic Ga plane underneath, and thereby ensure charge neutrality of the interface.

The areal density $N_{0,\mathrm{GaAs}}\cdot\lambda_{\mathrm{GaAs}}$ of interdiffused Zn acceptors in GaAs is higher for I and II than for III, which is

reasonable regarding that during a Zn-rich growth start Zn considerably diffuses into GaAs. λ_{GaAs} is 20 nm, in reasonable agreement with detailed studies on Zn diffusion in GaAs at higher temperatures.[31] For all three curves the segregation length k of iodine donors in ZnSe is taken as $k=25$ nm, consistent with ECV measurements on reference samples. The areal density of acceptors in ZnSe is 0 in I and II and is finite in III. This can be understood in terms of a replacement of As atoms by predeposited Se at the GaAs surface and their subsequent partial incorporation in the growing ZnSe layer as acceptors. In a Zn-rich growth start this As replacement is largely prevented. Such a complex growth start mechanism may also affect the MBE growth rate in the early stages of growth and thereby cause the significantly reduced total layer thickness for longer Se predeposition (compare Table I). A reduced growth rate for several minutes after growth start was also directly observed by *in situ* XRD studies of ZnSe/GaAs heteroepitaxy.[32]

In this section we have shown that our experimental values for the potential barrier height, the individual depletion widths and the electron deficit at ZnSe/GaAs heterointerfaces can be consistently modeled using reasonable parameters for band offsets, interface state density, atomic interdiffusion, and segregation of dopants.

Our observation of a reduction in the CBO with Se predeposition may seem in contrast to literature results. For ZnSe growth with a wide range of Zn/Se flux ratios, a reduction in the VBO with increasing Se flux was reported.[4] For comparing these studies with ours, it should be noted that two strongly different growth procedures were applied: (i) in our case ZnSe epilayer growth with a fixed Zn/Se flux ratio, optimized for structural quality and transport properties. Our only variable parameter was the amount of predeposited elementary Zn or Se at the interface prior to the ZnSe epilayer growth start; (ii) in Ref. 4 growth of interface and ZnSe epilayer with a constant Zn/Se beam pressure ratio (BPR), which was varied in a wide range ($0.1 < \mathrm{BPR} < 10$).

These different procedures with their specific growth kinetics in terms of, e.g., interdiffusion and desorption may well lead to different atomic configurations at the interface. From theoretical modeling it was shown that different interface configurations with comparable formation energy exist, which have opposing electric dipole moments, i.e., different CBO values.[3] Furthermore, it should be noted that the VBO for close-to-stoichiometric ZnSe growth start conditions in Ref. 4 is 0.98 ± 0.14 eV, which corresponds to a CBO $= 0.32 \pm 0.14$ eV. This value fits well between our results for Zn predeposition (sample B) and the lowest Se predeposition (sample C).

A more detailed quantitative comparison of our results, derived essentially from transport experiments on doped "thick-layer" heterostructures, with literature VBO values, derived from photoemission spectroscopy on extremely thin epitaxial layers, is hampered by possible additional, process-dependent sample properties, such as densities of dopants and defects, or a reduced effective ZnSe band gap at the interface. The impact of these effects may be quite specific for the various experimental methods. Therefore, for this purpose a combined analysis of the same samples first by electron photoemission spectroscopy and subsequently by our characterization methods after ZnSe overgrowth would be required for the various growth start procedures.

VII. CONCLUSION

We have studied the electronic and structural properties of MBE-grown n-type ZnSe/GaAs (001) heterointerfaces, a prototype of heterovalent semiconductor interfaces, and their variation with predeposition of Zn or Se in the fractional monolayer range at ZnSe growth start. Temperature-dependent I-V measurements across the heterointerfaces show that the potential barrier in the conduction band is reduced from about 550 meV for a very Zn-rich growth start, to 73 meV for our highest Se coverage. Based on the symmetry of I-V curves, we attribute this to a reduction in the ZnSe/GaAs conduction-band offset by an electric interface dipole moment. The lower offset manifests itself in a drastically reduced resistivity of the interface. Independent of the growth start ECV shows a carrier depleted region of about 50 nm width at the heterointerface with a constant electron deficit of 1.5×10^{13} cm^{-2} while Raman spectroscopy measurements reveal that the depletion region is partially shifted from GaAs to ZnSe with Se predeposition.

Taking account of a variable band offset, interface state density, atomic interdiffusion, and segregation is necessary to give a detailed description of the band bending and carrier distribution at heterovalent heterointerfaces. The effects of variable band offsets and interdiffusion leading to compensation or doping at the interface are general properties of heterovalent heterointerfaces. The extent of these effects depends on the material combination, epitaxial growth conditions, and especially on the sequence of the molecular deposition.

ACKNOWLEDGMENTS

We gratefully acknowledge continuous support by L. W. Molenkamp and valuable discussions with F. Reinert. This work was financially supported by the German BMBF within NanoQUIT project under Grant No. 01BM472, and by DFG under SPP-1285.

[1] A. Franciosi and C. G. van de Walle, Surf. Sci. Rep. **25**, 1 (1996).
[2] H. Farrell, M. C. Tamargo, J. L. de Miguel, F. S. Turco, D. M. Hwang, and R. E. Nahory, J. Appl. Phys. **69**, 7021 (1991).
[3] A. Kley and J. Neugebauer, Phys. Rev. B **50**, 8616 (1994).
[4] R. Nicolini *et al.*, Phys. Rev. Lett. **72**, 294 (1994).
[5] A. Colli, E. Carlino, E. Pelucchi, V. Grillo, and A. Franciosi, J. Appl. Phys. **96**, 2592 (2004).

[6] L. Kassel, J. W. Garland, P. M. Raccah, M. A. Haase, and H. Cheng, Semicond. Sci. Technol. **6**, A146 (1991).
[7] A. Frey, F. Lehmann, P. Grabs, C. Gould, G. Schmidt, K. Brunner, and L. W. Molenkamp, Semicond. Sci. Technol. **24**, 035005 (2009).
[8] A. Ishibashi, J. Cryst. Growth **159**, 555 (1996).
[9] F. Fischer *et al.*, J. Appl. Phys. **84**, 1650 (1998).
[10] C. C. Chu, T. B. Ng, J. Han, G. C. Hua, R. L. Gunshor, E. Ho, E. L. Warlick, L. A. Kolodziejski, and A. V. Nurmikko, Appl. Phys. Lett. **69**, 602 (1996).
[11] T. Yao *et al.*, Phys. Status Solidi B **202**, 657 (1997).
[12] A. Ohtake, S. Miwa, L. Kuo, T. Yasuda, K. Kimura, C. Jin, and T. Yao, J. Cryst. Growth **184-185**, 163 (1998).
[13] R. Fiederling, M. Keim, G. Reuscher, W. Ossau, G. Schmidt, A. Waag, and L. W. Molenkamp, Nature (London) **402**, 787 (1999).
[14] M. Ghali, R. Arians, T. Kümmell, G. Bacher, J. Wenisch, S. Mahapatra, and K. Brunner, Appl. Phys. Lett. **90**, 093110 (2007).
[15] A. A. Toropov, I. V. Sedova, S. V. Sorokin, Ya. V. Terent'ev, E. L. Ivchenko, and S. V. Ivanov, Phys. Rev. B **71**, 195312 (2005).
[16] A. A. Toropov, I. V. Sedova, S. V. Sorokin, Ya. V. Terent'ev, E. L. Ivchenko, D. N. Lykov, S. V. Ivanov, J. P. Bergman, and B. Monemar, Phys. Status Solidi B **243**, 819 (2006).
[17] H. H. Farrell and C. J. Palmstrom, J. Vac. Sci. Technol. B **8**, 903 (1990).
[18] D. Li and M. D. Pashley, Phys. Rev. B **49**, 13643 (1994).
[19] P. Kidd, P. F. Fewster, and N. L. Andrew, J. Phys. D **28**, A133 (1995).
[20] H. R. Ress, W. Spahn, R. Ebel, J. Nürnberger, M. Keller, H. Schäfer, M. Korn, M. Ehinger, W. Faschinger, and G. Landwehr, J. Cryst. Growth **184/185**, 90 (1998).
[21] S. M. Sze and K. K. Ng, *Physics of Semiconductor Devices* (Wiley, New York, 2007).
[22] A. C. Gossard, W. Brown, C. L. Allyn, and W. Wiegmann, J. Vac. Sci. Technol. **20**, 694 (1982).
[23] O. Chretien, R. Apetz, A. Souif, and L. Vescan, Thin Solid Films **294**, 198 (1997).
[24] H. Kroemer, Wu-Yi Chien, J. S. Harris, and D. D. Edwall, Appl. Phys. Lett. **36**, 295 (1980).
[25] G. Abstreiter, M. Cardona, and A. Pinczuk, Top. Appl. Phys. **54**, 5 (1983).
[26] D. E. Aspnes and A. A. Studna, Phys. Rev. B **27**, 985 (1983).
[27] J. Geurts, Surf. Sci. Rep. **18**, 1 (1993).
[28] S. Birner, T. Zibold, T. Andlauer, T. Kubis, M. Sabathil, A. Trellakis, and P. Vogl, IEEE Trans. Electron Devices **54**, 2137 (2007).
[29] U. Rössler, *Semiconductors*, Landolt-Börnstein, New Series, Group III Vol. III (Springer, New York, 1999).
[30] I. Vurgaftman, J. R. Meyer, and L. R. Ram Mohan, J. Appl. Phys. **89**, 5815 (2001).
[31] H. C. Casey, *Atomic Diffusion in Semiconductors* (Plenum Press, New York, 1973).
[32] A. Benkert, C. Schumacher, K. Brunner, and R. B. Neder, Appl. Phys. Lett. **90**, 162105 (2007).